Role of the Russell–McPherron effect in the acceleration of relativistic electrons

R.L. McPherron [a,*], D.N. Baker [b], N.U. Crooker [c]

[a] *University of California Los Angeles, Institute Geophysics and Planetary Physics, Los Angeles, CA 90095-1567, USA*
[b] *University of Colorado at Boulder, Laboratory for Atmospheric and Space Physics, 1234 Innovation Drive, Boulder, CO 80309-7814, USA*
[c] *Boston University, Center Space Physics, 725 Commonwealth Avenue, Boston, MA 02215, USA*

ARTICLE INFO

ABSTRACT

While it is well known that high fluxes of relativistic electrons in the Earth's radiation belts are associated with high-speed solar wind and its heightened geoeffectiveness, less known is the fact that the Russell–McPherron (R–M) effect strongly controls whether or not a given high-speed stream is geoeffective. To test whether it then follows that the R–M effect also strongly controls fluxes of relativistic electrons, we perform a superposed epoch analysis across corotating interaction regions (CIR) keyed on the interfaces between slow and fast wind. A total of 394 stream interfaces were identified in the years 1994–2006. Equinoctial interfaces were separated into four classes based on the R–M effect, that is, whether the solar wind on either side of the interface was either (geo)effective (E) or ineffective (I) depending on season and the polarity of the interplanetary magnetic field (IMF). Four classes of interface identified as II, IE, EI, and EE are possible. The classes IE and EI correspond to CIRs with polarity changes indicating passage through the heliospheric current sheet. To characterize the behavior of solar wind and magnetospheric variables, we produced maps of dynamic cumulative probability distribution functions (cdfs) as a function of time over 10-day intervals centered on the interfaces. These reveal that effective high-speed streams have geomagnetic activity nearly twice as strong as ineffective streams and electron fluxes a factor of 12 higher. In addition they show that an effective low-speed stream increases the flux of relativistic electrons before the interface so that an effective to ineffective transition results in lower fluxes after the interface. We conclude that the R–M effect plays a major role in organizing and sustaining a sequence of physical processes responsible for the acceleration of relativistic electrons.

© 2009 Elsevier Ltd. All rights reserved.

1. Introduction

1.1. Relativistic electrons

Early in the space era one of the first polar orbiting spacecraft 1963 38C revealed the presence of a 27-day periodicity in the flux of relativistic electrons ($E > 1.2$ MeV) at radial distances larger than 3 Re. Williams (1966) correlated temporal profiles of electron intensity from this spacecraft with the newly discovered interplanetary magnetic field (IMF) sector structure (Ness and Wilcox, 1965). He demonstrated that peaks in intensity occurred at or a little after the sector crossings, but only at boundaries where the IMF switched from negative (toward Sun) to positive (away from Sun). Wilcox and Ness (1965) had demonstrated that many solar wind parameters including velocity, field strength, density, as well as geomagnetic activity were organized by sector boundaries.

Based on these results Williams explained the intensity peak after the − to + transitions as a consequence of a peak in the Alfvén Mach number of the solar wind that occurred at only these times.

Eleven years later Paulikas and Blake (1979) studied the behavior of relativistic electrons at synchronous orbit near solar minimum and found that flux increases were highly correlated with solar wind speed and the IMF sector structure. Specifically they found that the electron fluxes begin to increase about a day after arrival of the high-speed stream and reach their maximum about 2–3 days later. They also noted: "A well-ordered stream pattern gives rise to a regular sequence of electron flux growth and decay …" Furthermore, they observed larger increases in fall for away sectors and in spring for toward sectors. They speculated that the Russell–McPherron (R–M) effect (Russell and McPherron, 1973) could explain this dependence on IMF sector structure. Baker et al. (1986) called attention to the fact that the high-speed solar wind is associated with corotating interactions regions (CIR) during the declining phase of the solar cycle and speculated that a pair of CIRs might form a "wave guide" allowing Jovian electrons to reach Earth. Subsequently, Baker et al. (1989) presented

* Corresponding author. Tel.: +1 818 8876220
E-mail addresses: rmcpherron@igpp.ucla.edu (R.L. McPherron),
daniel.baker@lasp.colorado.edu (D.N. Baker), crooker@bu.edu (N.U. Crooker).

evidence that the acceleration of electrons to relativistic energies is an internal magnetospheric process.

Nagai (1988) demonstrated the truth of the previous suggestion with synchronous observations of relativistic electron fluxes and magnetic indices. Using superposed epoch analysis he showed that electron fluxes reach a minimum at the time of minimum Dst and maximum Kp. He then demonstrated that a linear prediction filter with Kp as input can predict more that half the variance of the daily average flux. These results suggested the possibility that stronger activity, i.e. magnetic storms, would produce larger fluxes of relativistic electrons. Note, however, that Baker et al. (1990) showed that the solar wind speed is an equally good predictor of electron fluxes, and that AE does not do as well as speed or Kp. Later Reeves (1998) explicitly considered the possibility that magnetic storms are responsible for the acceleration of relativistic electrons. He concluded that more than a storm is needed.

> "… but that there is some additional factor, either in the solar wind or in the magnetosphere, that determines whether a given storm will produce relativistic electrons or not and how strong that response will be."

O'Brien et al. (2001a) examined a very large set of magnetic storms and found that the best predictors of high fluxes are solar wind speed >450 km/s, Pc 5 wave power >1000 nT^2 and long duration of the storm recovery phase. The strength of the ring current was not a good predictor. Reeves et al. (2003) examined this question further finding that only half of all storms accelerate electrons and that the ratio of pre- to post-storm fluxes is nearly independent of the strength of storms. They conclude:

> "However, for all solar wind velocities both increases and decreases were still observed. Our analysis suggests that the effect of geomagnetic storms on radiation belt fluxes are a delicate and complicated balance between the effects of particle acceleration and loss."

In this paper we will demonstrate that previously neglected factors include season and polarity of the interplanetary magnetic field.

With the advent of long duration spacecraft missions it became possible to perform more detailed analysis of the temporal properties of relativistic electrons. Baker et al. (1999b) demonstrated that electron fluxes measured by both the low-altitude SAMPEX satellite, and the high-altitude Polar spacecraft exhibit very pronounced semiannual variations of electron fluxes. Using quarterly averages centered on the equinoxes and solstices they found that fluxes were nearly 3 times higher at the equinoxes than at the solstices. They attributed this to the Russell–McPherron effect but noted the modulation of electron fluxes was much stronger than it is for geomagnetic activity. In discussing their result they called attention to the fact that the correlation of electron fluxes with solar wind velocity might indicate that low-frequency ULF waves are produced by the Kelvin–Hemholtz (K–H) instability during high-speed streams (Rostoker et al., 1998). They therefore suggested the following model to explain the observations.

During the declining phase of the solar cycle large coronal holes produce high-speed solar wind streams. When these streams hit Earth they cause substorms when the IMF is southward in gsm coordinates as a consequence of the Russell–McPherron effect and other factors. The substorms inject seed populations of low-energy electrons into the inner magnetosphere. ULF waves in the Pc 5 band produced by the K–H instability radially diffuse the electrons inward increasing the electron energy to relativistic values.

Current ideas about electron acceleration are more sophisticated (Horne et al., 2006) but do not deal directly with the topic of this paper—the role of the Russell–McPherron effect. In the following we use data from two solar cycles to demonstrate that the basic idea proposed by Baker et al. is correct, but there are additional factors associated with corotating interaction regions that need to be considered. We begin with a review of the Russell–McPherron effect.

1.2. The Russell–Mcpherron effect

In the early 1970s the concept of magnetic reconnection as the cause of geomagnetic activity was not universally accepted. Consequently it was important to examine implications of the hypothesis and determine if they were supported by data. To this end Russell and McPherron (1973) noted that the semiannual variation of geomagnetic activity with peaks at the equinoxes might be explained by magnetic reconnection. Their argument was geometrical and is illustrated in Fig. 1. At the top left of the figure the circle represents the orbit of the Earth around the Sun in the ecliptic plane. The Earth is shown at spring equinox on 21 March. At this time the rotation axis of the Earth is pointed $23.44°$ away from its orbital velocity vector and is orthogonal to the Earth–Sun line. A few weeks earlier (5 March) the rotation axis of the Sun is tilted directly away from Earth so that Earth is located at $7.25°$ south heliographic latitude. The interplanetary magnetic field generally lies in the solar equatorial plane and is wrapped into a spiral as a consequence of the radial flow of the solar wind and the rotation of the Sun. The geocentric solar ecliptic (gse) coordinate system is shown in the lower left of the figure. This coordinate system is centered in the Earth with the X-axis always pointing directly to the center of the Sun. The Z-axis points to the north ecliptic pole and the Y-axis is orthogonal to both, and antiparallel to Earth's orbital velocity. A spiral magnetic field toward the Sun as shown in the top panel is depicted by the vector labeled "Toward". Note that this vector has a negative projection on the gse Y-axis. The bottom right panel shows the geometry as viewed along the gse X-axis toward the Sun. The
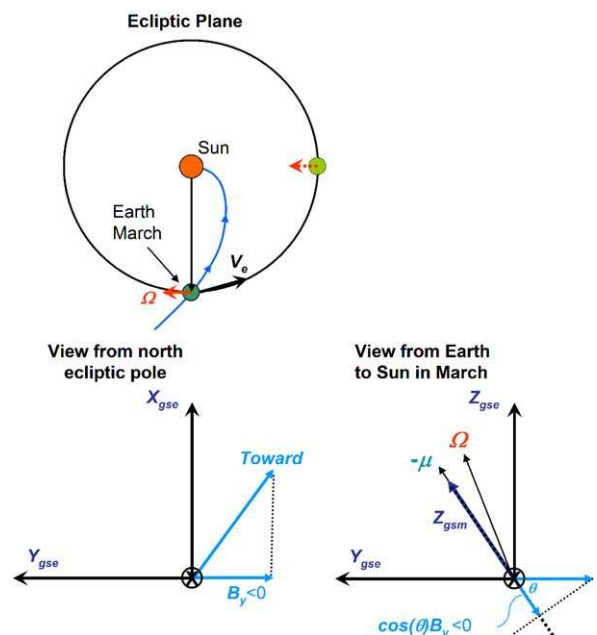

Fig. 1. An illustration of the geometry of the spiral magnetic field of the solar wind and how it is converted to a geomagnetically effective southward component at Earth at spring and fall equinox.

Earth's rotation axis is tilted 23.44° away from Z toward the Y-axis. At 2247 UT on 19 March the dipole axis lies in the Y–Z plane at an angle of 34.8° to the Z-axis. The projection of the Y-component of the spiral magnetic field onto the direction of the dipole is negative and magnetic reconnection between the IMF and the dipole magnetic field is expected. Reconnection drives internal flows in the magnetosphere and produces magnetospheric substorms responsible for geomagnetic activity.

It has been found that phenomena within the magnetosphere are generally controlled by the orientations of the Sun vector and the dipole axis. The geocentric solar magnetospheric (gsm) coordinate system is defined in terms of these two vectors. X points to the Sun as in gse coordinates. The Z-axis is orthogonal to X but is rotated about X so that the dipole always lies in the X–Z plane. At the time assumed in the drawing the dipole and gsm Z-axis are coincident. At other times the dipole will lie in front or behind the gsm Y–Z plane. As Earth rotates and progresses around the Sun the relative orientation of these coordinates systems change. For example, at summer solstice (second ball in top panel) Earth's rotation axis lies in the gse X–Z plane and an ecliptic IMF will have no projection onto the gsm Z-axis. Thus no magnetic activity is expected as a result of geometric projection effects.

At fall equinox the gse coordinate system has rotated 180° about the ecliptic pole. At this time only "Away" sectors of the IMF will project onto the gsm Z-axis with a negative projection. Also, the universal time of maximum dipole tilt away from the gse Z-axis is ~12 h later (1032 UT on 22 September). These facts lead to the Russell–McPherron rule "Spring To Fall Away" as the orientation of the IMF that produce geomagnetic activity at Earth.

This entire argument is made more complicated by the tilt of the Sun's rotation axis because the spiral IMF actually lies in the solar equatorial plane. Another coordinate system is needed to describe this fact (geocentric solar equatorial or gseq). This difference changes the day and universal time at which the maximum projection of the spiral IMF occurs at Earth. The spring peak actually occurs at 22:35 on 7 April and the fall peak at 10:20 on 11 October. A second complication arises from the fact that in general slow-speed solar wind originates near the solar magnetic equator while high-speed solar wind comes from higher and lower heliographic latitudes (Phillips et al., 1995). It is possible that activity at the equinox is enhanced by a high solar wind velocity rather than the R–M effect. This suggestion is know as the "axial effect" (Cliver et al., 2000). A third complication is the argument by Cliver et al. (2000) that the coupling efficiency between the solar wind and Earth is reduced at solstices relative to that at equinox because the angle in the X–Z plane between the solar wind velocity and the Earth' dipole is not 90°. Paradoxically this is named the "equinoctial hypothesis".

Of central importance to this paper is the fact that the Russell–McPherron effect is not some secondary seasonal effect but rather a primary effect in determining whether or not a high-speed stream will be geoeffective. Fig. 2 illustrates this property. It shows speed profiles of the two streams of opposite magnetic polarity that swept past Earth with every solar rotation during 1974. It was data from this period that led to our current understanding of stream and magnetic sector structure in terms

of solar dipolar fields tilted with respect to the ecliptic plane during the declining phase of the solar cycle (e.g., Hundhausen, 1977). Because subsequent solar cycles brought more complicated patterns, data from 1974 remain the best source for illustrating the magnetospheric response to high-speed streams of opposite polarity. In particular, Fig. 2 shows what is considered to be the classical Dst profile in response to the second stream. The storm index dips sharply as speed rises in the compressed interaction region and then settles to a level of lesser activity that lasts for nearly half the solar rotation. In contrast, Dst is barely depressed during passage of the first stream. The stark difference in response can be ascribed to the Russell–McPherron effect. The data are from a period near northern spring equinox, when magnetic fields pointing toward (away from) the Sun, ordered in heliographic coordinates, project a southward (northward) component in magnetospheric coordinates, which increases (decreases) geomagnetic effectiveness. Thus, the stream with toward polarity produced the classical recurrent storm profile while the stream with away polarity did not. This strong control by the Russell–McPherron effect can be seen throughout 1974 in the 27-day recurrence plot of Dst in Crooker and Siscoe (1986).

The fact that some high-speed streams produce classical recurrent storms while others do not, depending upon season and magnetic polarity, strongly impacts patterns of relativistic electron occurrence in the magnetosphere. This paper reports on the results of a rigorous analysis that confirms that impact.

1.3. Database and event selection

The data used in this study have been acquired over a long period of time by downloading data from National data centers, project data bases, and other government agencies. The database includes all solar wind plasma and magnetic field measurements from the space age (1964–2007). These data have been interpolated to 1-min resolution and propagated to the subsolar bow shock using the Modified Minimum Variance Method developed by Weimer and others (Bargatze et al., 2005; Haaland et al., 2006a, b; Weimer et al., 2003; Weimer, 2004). Other data include synchronous electron data from DOE and NOAA spacecraft operated by LANL and NOAA, synchronous magnetometer data from GOES spacecraft, ULF wave data from InterMagnet stations, and magnetic indices from several data centers. These data are currently being migrated to the NASA Virtual Magnetospheric Observatory at UCLA and will soon be publicly available. Table 1 summarizes the data used in this study.

Events are defined as Earth passage of corotating interaction regions. The time assigned to these events is the stream interface defined by a zero crossing of the azimuthal flow angle of the solar wind. The procedure for this selection is described in greater detail in Section 2. We have identified a total of 394 stream interfaces in the years 1995–2006 during which we have virtually continuous solar wind plasma and magnetic field data. This interval covers most of the declining phases of solar cycles #22 and #23. A list of all stream interfaces is available on request.

The measure of the flux of relativistic electrons used in this paper is the proxy noon flux at synchronous orbit. The derivation of this quantity is discussed below in Section 2.10.

2. Experimental results

2.1. Association of relativistic electrons with solar wind and IMF

In Section 1, we reviewed a few previous studies of relativistic electrons and noted the correlations of electron flux with solar
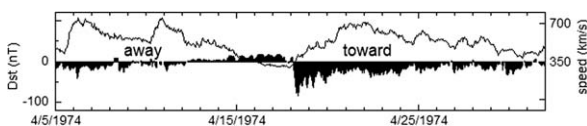

Fig. 2. Time variations of solar wind speed and the Dst index of geomagnetic activity during passage of two high-speed streams of opposite polarity. The stream with toward polarity is strikingly more geoeffective owing to the Russell–McPherron effect (after Crooker and Siscoe, 1986).

Table 1
Data types, source of data, and time intervals covered by different types..

| Data type	Source	Time interval
AE indices	WDC for Geomagnetism Kyoto http://swdcwww.kugi.kyoto-u.ac.jp/wdc/Sec3.html	1994–2007 except 1996
Asym-Sym indices	WDC for Geomagnetism Kyoto http://swdcwww.kugi.kyoto-u.ac.jp/wdc/Sec3.html	1981–2005
Pc 5 power index	space.augsburg.edu, in the folder: /MACCS/ULF_Index/	1994–2003
Solar wind & IMF from wind & ACE	NSSDC http://cdaweb.gsfc.nasa.gov/istp_public/	1994–2008
GOES electrons >2 MeV (#/cm^2/s/s)	paul.obrien@aero.org reeves@lanl.gov	1989–2000
GOES-8 electrons >2 MeV (#/cm^2/s/s)	NSSDC http://cdaweb.gsfc.nasa.gov/istp_public/	1995–2003
GOES-12 electrons >2 MeV (#/cm^2/s/s)	NSSDC http://cdaweb.gsfc.nasa.gov/istp_public/	2003–2005
Stream interface list	rmcpherron@igpp.ucla.edu	1994–2008
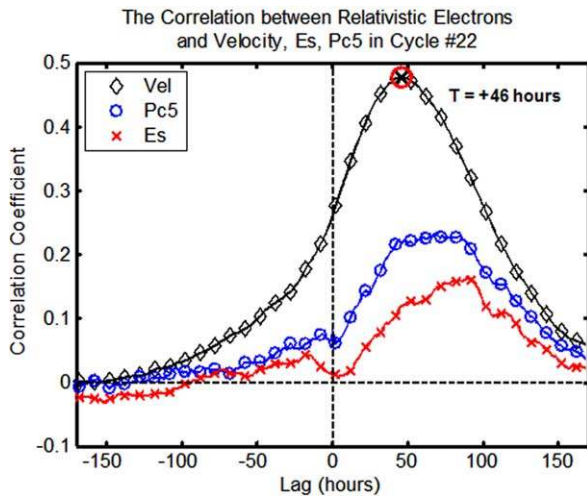
Fig. 3. The correlations between noon flux of relativistic electrons at synchronous orbit and several important variables are plotted as a function of lag in hours. Electron fluxes reach peak values 46 h (∼2 days) later than the velocity (black diamonds). Pc 5 waves in the magnetosphere have the next best correlation with electrons (blue circles) followed by the southward component of the electric field (red x). (For interpretation of the references to color in this figure legend, the reader is referred to the web version of this article.)

Fig. 4. The semiannual variation of the flux of relativistic electrons at synchronous orbit during sunspot cycle #22 is illustrated by the median of the flux ratio as a function of time relative to summer solstice (dashed black line). The flux ratio is defined as the 27-day running average time series of synchronous noon flux divided by 365-day running averages of this flux. The solar wind velocity does not show a similar modulation as demonstrated by the shaded band near a ratio of 1.0.

wind velocity, substorm activity, and ULF waves. These correlations are illustrated in Fig. 3 using 11 years of data. The best linear correlation is between log electron flux with $E > 2$ MeV and solar wind speed. The peak electron flux occurs 2 days after a peak in velocity (black diamonds). Pc 5 wave power is the second most important variable as shown by the curve denoted by blue circles. Es, the solar wind electric field calculated from solar wind speed and the southward component of IMF Bz, displays the lowest correlation and the longest delay. The results seem to suggest that variations in electron fluxes are preceded first by Es, i.e. substorms, then ULF waves, and finally solar wind velocity.

2.2. Semiannual variation of geosynchronous fluxes

Previous work has shown that fluxes of relativistic electrons display a very strong semiannual variation (Baker et al., 1999a; Li et al., 2001). This fact is illustrated in Fig. 4. The dashed line is a median ratio calculated from an ensemble of 11 years of proxy noon electron fluxes at synchronous orbit during solar cycle #22. The reference time for the superposed epoch analysis is summer solstice. The quantity analyzed is the ratio of a 27-day running average of the fluxes to a 365-day running average. This ratio removes a very strong dependence of average fluxes on the solar cycle and isolates the semiannual variation. Note there are strong peaks in electron fluxes close to the equinoxes and minima near
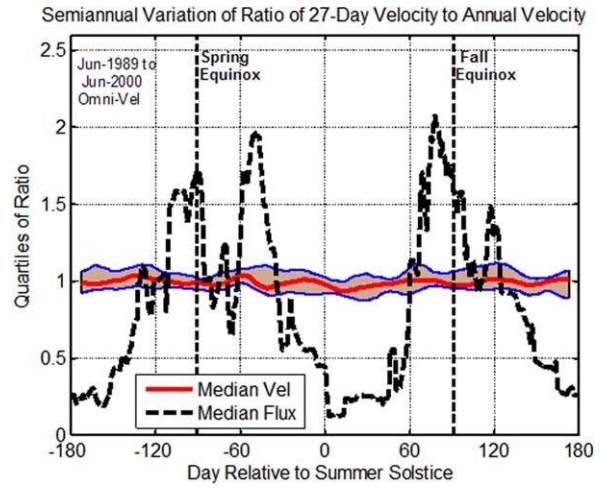
the solstices. A brown patch and heavy red line behind the dashed line show the results of a similar analysis of the solar wind velocity. Clearly there is no evidence of a semiannual variation in solar wind velocity so we can dismiss the axial hypothesis that changes in Earth's heliographic latitude and hence of solar wind velocity is the cause of the semiannual variation of electron fluxes.

2.3. Solar cycle variation of electron flux

The flux of energetic electrons reach a maximum in the declining phase of the solar cycle as demonstrated in Fig. 5. The top panel presents daily averages (red) and 27-day running averages (blue) of the flux measured at various GOES spacecraft at 135° west longitude (O'Brien et al., 2001a). The second panel displays sunspot number treated in a similar manner. The minimum of this cycle occurred in October 1996. The bottom panel compares 27-d running averages from the top two panels. It is obvious that the relativistic electrons reach a maximum in the declining phase 2–3 years before solar minimum. It is well known that this is the time of recurrent high-speed streams commonly referred to as corotating interaction regions (CIR) (Forsyth and Marsch, 1999; Gosling et al., 1978a; Hundhausen, 1977).

The characteristics of relativistic electrons displayed in the preceding figures lead us to consider high-speed streams or CIRs as an important factor in the acceleration of relativistic electrons. The pronounced semiannual variation of fluxes suggests that we consider the role of the Russell–McPherron effect as well.
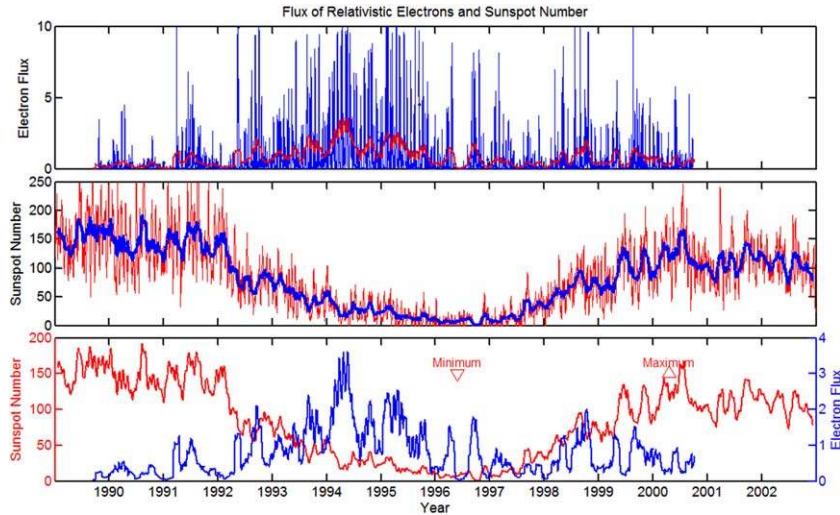
Fig. 5. The occurrence of relativistic electrons during sunspot cycle 22 is shown here. The top panel displays the flux of electrons 1.8–3.5 MeV ($\#/cm^2/s/sr/keV$) measured by LANL spacecraft at synchronous orbit. The blue trace shows daily averages while the red line shows 27-day running average. The middle panel presents daily (red) and 27-day running averages of sunspot number (blue). The bottom panel compares 27-day running averages. Solar minimum occurred in late 1996. (For interpretation of the references to color in this figure legend, the reader is referred to the web version of this article.)
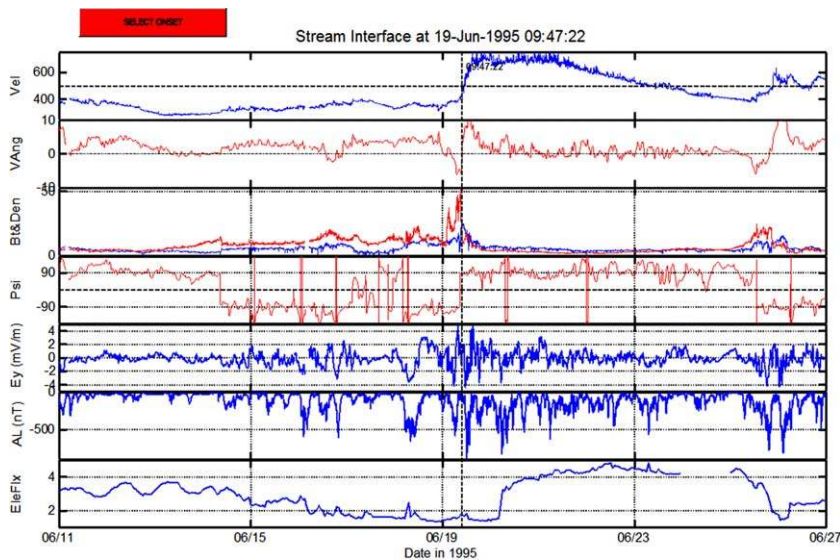

Fig. 6. An example of the interactive selection of the time of the interface between a low- and high-speed solar wind stream is presented. From the top down the panels show speed, azimuthal flow angle, density and total field, spiral angle of the IMF, GSM Ey, AL index, and flux of relativistic electrons at synchronous orbit. The zero crossing of the azimuthal flow angle is the reference time selected.

2.4. Identification of stream interfaces

Stream interfaces are the two-dimensional contact between the low-speed gas emitted from the streamer belt on the Sun and a high-speed stream emitted from a coronal hole (Gosling et al., 1978b; Gosling and Pizzo, 1999). The interface is defined by a variety of characteristics including compression and flow deflection. An example interface is presented in Fig. 6. The top panel presents the solar wind velocity with a vertical dashed line defining the time of the interface. The velocity is less than 400 km/s in the slow stream before the interface and rises to more than 600 km/s after the interface. The second panel shows the azimuthal flow angle of the solar wind in the ecliptic plane. A short time before the interface the flow is deflected to the west of radial (as seen from the Northern Hemisphere of Earth looking toward the Sun). After the interface the flow is deflected to the

east. The time of the zero crossing of the azimuthal flow angle is taken as the time of the interface.

The third panel presents the solar wind density (red) and total magnetic field (blue). The density rises before the interface and then drops suddenly at the interface. The magnetic field also reaches a peak near the interface, usually a little after. The fourth panel displays the spiral angle of the IMF in the ecliptic plane in a coordinate system rotated $45°$ (counter clockwise) around the gse Z-axis. In this system a "Toward" sector is at an angle close to $-90°$ and an "Away" sector is close to $+90°$. Many stream interfaces are preceded by an IMF sector crossing defined as a reversal of the spiral angle. The fifth panel displays the GSM Ey component of the IMF (note we have reversed the sign of Ey to correspond to Bz). This is the geoeffective component that drives magnetic activity. An important characteristic of high-speed streams is that they contain low frequency, irregular Alfvén waves

propagating away from the Sun (Roberts and Goldstein, 1990; Tsurutani and Gonzalez, 1987). These waves appear as large fluctuations in Bz (or in Ey) after the interface. Each southward turning of the IMF caused by a wave drives geomagnetic activity. The fact that Bz is multiplied by the speed in Ey amplifies the importance of these waves after the interface. The effect of the transition from slow to high-speed solar wind in the AL index is illustrated in panel 6. Auroral zone geomagnetic activity is stronger and more frequent after the interface than it is before.

The bottom panel displays the association of relativistic electrons at synchronous orbit with this stream interface. Five days before the interface the electron fluxes were dropping slowly eventually reaching a level close to background. After the interface they increased for several days to a value nearly four orders of magnitude higher than the minimum before the

interface. As we show below the average behavior of electron fluxes is generally not so extreme.

2.5. Analysis method

The method used in our analysis is illustrated by Fig. 7, which shows the average velocity profile relative to a stream interface for all 394 stream interfaces in the interval 1995–2006. To obtain these results velocity data for each interface was placed in successive rows of an ensemble matrix containing 10 days of data centered on the time of the interface. A window of width 15 samples was moved across the matrix and all data points from all rows were used to calculate a cumulative probability distribution (cdf). The cdfs were interpolated to a uniform grid and then mapped with contours (thin black lines) and color change at the deciles of the cdf. Heavy lines in the map are the quartiles. In subsequent figures we utilize either the quartiles or the medians to summarize the results.

The map in Fig. 7 shows the typical behavior of solar wind speed relative to a stream interface. For 5 days preceding the interface speed decreases in the slow stream. About 12 h before the interface the speed begins to increase. This is slow-speed wind accelerated by the impact of the high-speed wind. At the interface speed reaches its peak rate of change. Within 24 h after the interface the speed reaches a maximum. This interval after the interface is the portion of the high-speed stream that has been decelerated by the interaction. The speed remains high for several days and then begins a slow decrease. The minimum median speed before an interface is 380 km/s and the median at the peak is 540 km/s. There is considerable variance about the median as evident from the deciles of the dynamic cumulative probability distribution.

2.6. Average solar wind and IMF behavior relative to stream interface

The average behavior of solar wind plasma and IMF parameters relative to all stream interfaces in the interval 1995–2006 is presented in Fig. 8. The left side of the figure displays parameters
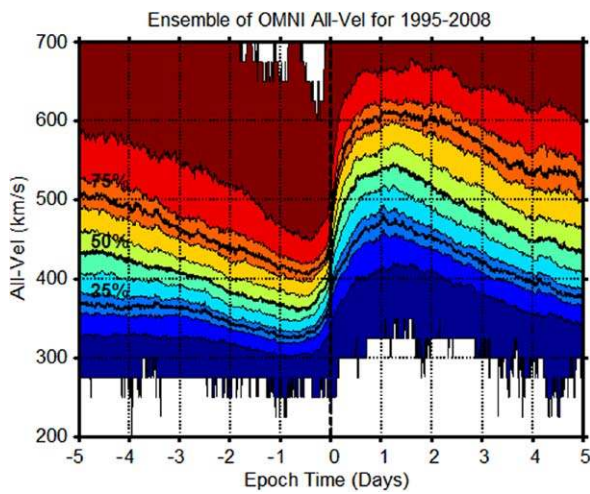

Fig. 7. A map of the dynamic cumulative probability distribution is presented. Thin lines and changes in color show the deciles of the distribution. Heavy lines are the quartiles. The time reference for this superposed epoch analysis is the zero crossing of the azimuthal flow angle at the center of a CIR.
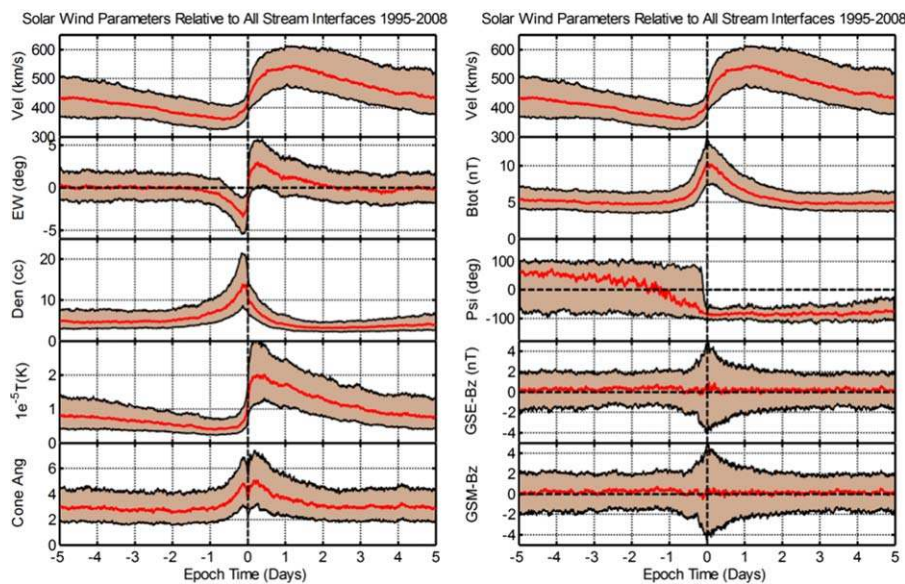

Fig. 8. The quartiles of various solar wind plasma and IMF parameters relative to all stream interfaces in the interval 1995–2006 are shown. Black lines define the upper and lower quartiles bounding the brown colored patches containing half of all events. The heavy red line is the median. The vertical dashed line is the time of the stream interface used in the superposed epoch analysis. Parameters shown on the left side of the figure include: velocity, azimuthal flow, density, temperature, cone angle (between IMF and Earth–Sun line). Parameters on the right side include: velocity, IMF magnitude, spiral angle (ψ) (rectified to have toward sectors after interface), Bz in gse and Bz in gsm coordinates. (For interpretation of the references to color in this figure legend, the reader is referred to the web version of this article.)

in the solar wind plasma and the right side shows parameters of the IMF. The average behavior is very similar to that discussed in terms of the specific example shown in Fig. 6. The plasma variations near the interface include a rapid rise in speed across the interface and a slow decay after; opposite deflections in flow before and after the interface with a zero crossing at the interface (by definition); a slow rise to a peak in density followed by a sharp drop; a rapid increase in temperature followed by slow decay, and a double peak in the cone angle of the flow around the Sun–Earth line. The IMF presented in the right panel rises rapidly to a peak in total field just after the interface followed by a slower decay; a sector boundary crossing generally occurs sometime before the interface (shown here for geoeffective high-speed streams portrayed as in spring); an increase in the amplitude of gse Bz fluctuations starting 12 h before that maximizes at the interface and then decays for 2 more days; gsm Bz fluctuations that are nearly the same as those in gse.

The organized behavior of the solar wind leads to organized behavior within the magnetosphere as demonstrated in Fig. 9. Panel 1 shows the speed for reference. Panel 2 shows that the power of ground ULF waves in the Pc 5 band ($T = 150–500\,\text{s}$) rises rapidly starting about 1 day before the interface. The power peaks a few hours after the interface, and then decays slowly for many days with a profile very similar to that of speed. The bottom panel shows the response of the ring current as measured by Sym-H index. There is a maximum in Sym-H a few hours before the interface caused by a peak in dynamic pressure at this time. This is followed by a rapid drop lasting about 12 h. The minimum of median Sym-H ($-22\,\text{nT}$) is not significant in terms of magnetic storm activity. In fact only 25% of the interfaces cause a decrease to less than $-40\,\text{nT}$. The fourth panel displays the response of the AE index. Auroral zone activity begins a few hours before the interface and peaks about 12 h after. However, elevated activity persists for many days afterwards.
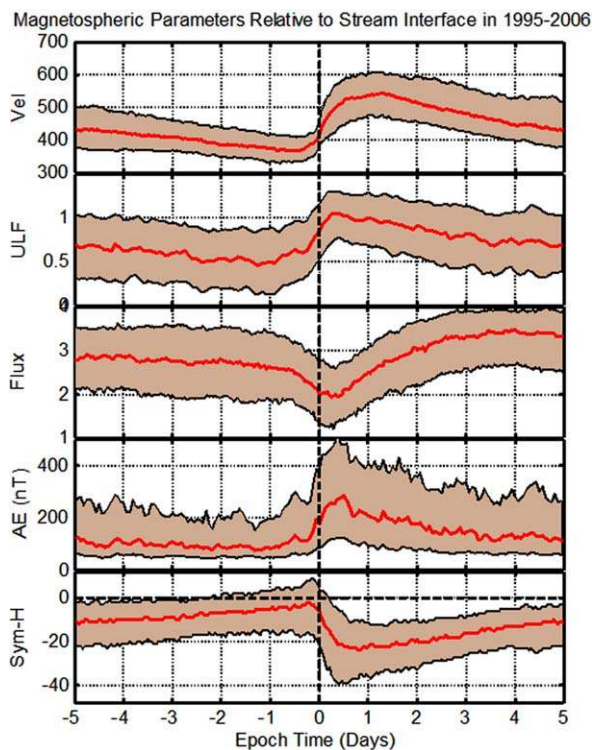

Fig. 9. A plot similar to Fig. 8 showing the relation of magnetospheric parameters to stream interfaces. The panels include: velocity, Pc 5 power on ground, log flux relativistic electrons, AE index and Sym-H.

The middle panel of Fig. 9 summarizes the behavior of the log flux of relativistic electrons relative to the interface. About 2 days before the interface the fluxes begin a gradual drop. Twelve hours before the interface they drop more rapidly reaching a minimum 6 h after the interface that is about a factor of 10 lower than their values several days before. After the interface the electron flux increases by $1\frac{1}{2}$ orders of magnitude reaching a peak 3–4 days after the interface. Subsequently they decay slowly.

From these data it is apparent that relativistic electrons at synchronous orbit rapidly disappear during the passage of a CIR (interface ±12 h). When Earth enters the high-speed stream a weak magnetic storm, substorm activity and ULF waves occur in the magnetosphere and electron fluxes rise to high levels. Electron disappearance is associated with the initial and main phases of the weak magnetic storm while electron enhancement is associated with the recovery phase. It should also be noted that the recovery phase is much longer than expected for typical storms. In association with the long decay of the AE activity this suggests that particle injection events are occurring for many days after the interface.

2.7. Classification of stream interfaces

Our goal in this paper is to examine the importance of the Russell–McPherron effect on the flux of relativistic electrons in Earth's magnetosphere. To do this we classified stream interfaces according to the Russell–McPherron rule "Spring To Fall Away". Regardless of speed we define a geoeffective solar wind stream as one which satisfies this rule. We expect that high-speed streams are likely to drive larger activity than low-speed streams because Ey = VBz is larger. The two streams and two states lead to four classes:

(1) ineffective slow-ineffective high (II)
(2) effective slow-effective high (EE)
(3) ineffective slow-effective high (IE)
(4) effective slow-ineffective high (EI)

The R–M rule only applies to the solar wind around equinox. In our analysis we have defined equinox broadly to maximize the number of events. Our definition includes 67 days either side of side of an equinox. In spring an IMF having a positive spiral angle between 0.0 and $+180°$ was classified ineffective while an IMF with negative spiral angle 0.0 to $-180°$ was classified as effective. In fall the definition is reversed. An interface was classified as "no change" (II or EE) when the median spiral angle had the same sign before and after the interface. A "change" interface required that the median angle change sign across the interface. Recall that we have defined spiral angle in a coordinate system rotated counter-clockwise about +Z gse by 45°.

2.8. Occurrences of stream interfaces

It is important to determine how frequently the various classes occur in the observations. Occurrence statistics are summarized in Table 2. In $11\frac{1}{2}$ years we identified a total of 394 stream interfaces corresponding to an average rate of 2.5 interfaces per solar rotation. The interfaces were almost uniformly distributed over the solar cycle with ~32 per year except for 1997 where we only identified 15 interfaces. Our definition of equinox put 150 of these interfaces in the spring category and 157 in the fall category, but only 44 and 43 interfaces, respectively around winter and summer solstice. Also our observations show that not all stream interfaces are preceded by an IMF sector crossing. With our definitions only 58% of the events had a sector crossing. It should be emphasized,

however, that our definition of a sector crossing requires that the 5-day means of the spiral angle before and after the interface differ by at least 90°. There are some events where a temporary crossing may have occurred but the "no sector crossing" interfaces on average have more than 75% of their values of the same sign before and after the interface.

Table 3 shows the distribution of these interfaces into the four classes defined by the Russell–McPherron effect in spring (first row) and fall (second row). In spring the four classes were relatively uniformly populated. However, in fall the ineffective to ineffective (II) situation occurred infrequently compared to spring,

Table 2
Number of stream interfaces at different times of year and with sector boundary crossings..

Category	Number
All	394
Spring	150
Fall	157
Winter	44
Summer	43
Sector cross	227
No sector cross	167

Table 3
Occurrences of various classes of stream interfaces defined according to the Russell–McPherron rule "Spring To Fall Away" in top two rows. The percentage of interfaces with flux increases before or flux decreases after an interface in middle two rows. The median decrease in log flux before and median increase after an interface is in last two rows..

	Ine–Ine	Ine–Eff	Eff–Ine	Eff–Eff
# Spring	38	44	35	33
# Fall	14	46	49	48
Med decrease before	0.46	0.64	0.97	0.44
Med increase after	0.88	1.83	0.78	1.37
% Increase before	26.2	16.1	12.0	29.9
% Decrease after	21.4	6.2	20.0	16.9

but the other three classes had more nearly the same occurrence frequency. The explanation of these results probably lies in the particular structure of the IMF and streams present during this solar cycle. What they imply is that the relation of streams and sectors was nearly random when averaged over the $11\frac{1}{2}$ years. In our analysis we found no obvious precursor for those stream interfaces that were preceded by a sector boundary crossing. This makes it difficult to use observations in the low-speed stream to predict whether the high-speed stream will be geoeffective. Of course if the transition (sector boundary crossing) is observed during a low-speed stream then forecasts based on the Russell–McPherron effect can be made.

2.9. Dependence of magnetospheric response on IMF polarity

In Section 1.2, we suggested that the semiannual variation of relativistic electron fluxes might be a consequence of the Russell–McPherron effect. To examine this possibility we defined four classes of stream interfaces corresponding to the nature of the transition in IMF sector structure that occurs just before a stream interface. These four classes were designated II, EE, IE, and EI where the first letter refers to the polarity of the low-speed stream according to the R–M rule (I for ineffective and E for effective) and the last letter to the polarity of the high-speed stream. We have carried out a superposed epoch analysis for these four classes and the results are presented in Figs. 10 and 11. Results for stream interfaces in which there was no well-defined sector crossing are summarized in Fig. 10. Panels on both sides of the figure present quartiles of IMF spiral angle (psi), gsm Ey, and the Sym-H index. On the left side we show the response for ineffective orientation of the IMF both before and after the interface. In creating the figure we reversed the sign of the spiral angles (psi) in fall to look like spring so that a positive value corresponds to an away sector which in spring is ineffective. The middle panels exhibit the result expected for Ey when selecting according to the Russell–McPherron effect. On the left ineffective low to ineffective high-speed streams have Ey in gsm coordinates biased positive as evident from the displacement of quartiles
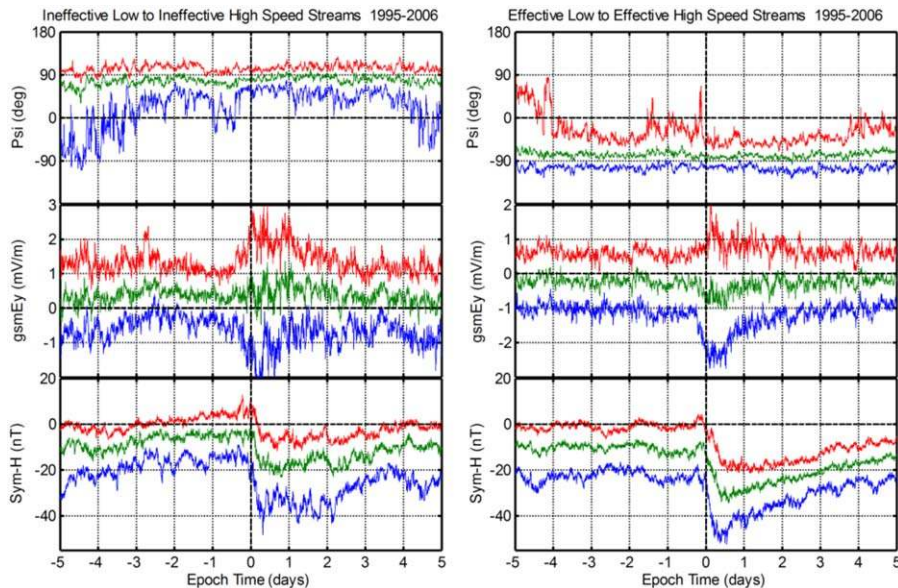

Fig. 10. The quartiles of the spiral angle (psi), Ey and Sym-H index as a function of epoch time are shown for two classes of CIR determined by Russell–McPherron rule: ineffective low speed to ineffective high speed (II), and effective low to effective high (EE). Note that the sign of psi has been revered in fall to correspond to spring. Also gsm Ey has been reversed to correspond to the sign of Bz so negative Ey implies geomagnetic activity.
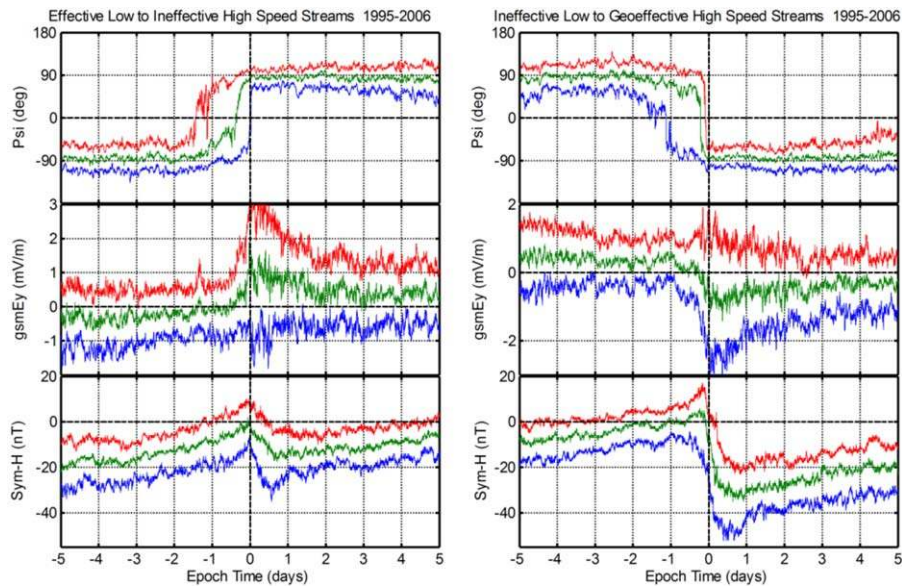
Fig. 11. Similar to Fig. 10 but for the R–M classes effective low to ineffective (EI) and ineffective low to effective high (IE).

relative to the zero line. [Note the sign of Ey is reversed to correspond to Bz.] On the right side effective low- and high-speed streams have Ey biased negative. The result of this bias is evident in the Sym-H index measuring magnetic storm activity plotted in the bottom panels. For a positive bias of gsm Ey the median Sym-H index is close to zero before the interface and only drops 15 nT after the interface. Although the profile has the classic form of a magnetic storm with initial, main, and recovery phases, it would not be classified as a magnetic storm since minimum median Sym-H > -30 nT, a value often used as a threshold for weak storms (Gonzalez et al., 1994). In the right panel, Sym-H is a little more negative before the interface and drops somewhat more reaching a minimum median of about -30 nT. Note for both classes a substantial number of the events show a strong negative bias in gsm Ey for about a day around the interface. It is this interval of more strongly southward IMF that causes the main phase development of these weak storms.

The behavior of the two classes of CIR having a sharp transition from one IMF sector to the other is displayed in Fig. 11. The left side shows changes from geoeffective behavior in the low-speed stream to ineffective behavior in the high-speed stream. Usually the spiral angle (top panel) reverses sometime between 1 and $1\frac{1}{2}$ days before the interface. However, at least one quarter of the events make the transition shortly after the interface. The middle panel displays the behavior of gsm Ey. The effective to ineffective (EI) transitions shown on the left have gsm Ey biased negative before the interface and positive after the interface. For this case ring current activity before and after the interface is close to being the same with only a slight increase in Sym-H due to high dynamic pressure at the interface. The situation is quite different for the ineffective to effective transition (IE). In this case gsm Ey in the right middle panel makes a transition from positive to negative just before the interface. The bottom panel shows a pronounced signature of a magnetic storm with an elevated initial phase and a rapid drop of 30 nT during the main phase. The recovery phase is long and protracted.

Note that the effective to ineffective transition (left panels) produces a strong positive bias in gsm Ey for about a day about the interface in more than half the events. Similarly, the ineffective to effective transition causes more than half the events to have a strong negative bias. The cause of this in not known but

it is important in the creation of geomagnetic activity at the interface.

It is evident from the preceding discussion that the geometry of the spiral IMF near equinox referred to as the Russell–McPherron effect significantly influences the gsm Ey responsible for the transport of magnetic flux to the dayside magnetopause. Four different classes of CIR depending on the orientation of the IMF in the two streams produce four different patterns of geomagnetic activity. We expect that this will be the case for relativistic electrons at synchronous orbit.

2.10. Response of relativistic electrons at synchronous orbit

The noon flux of relativistic electrons at synchronous orbit has been obtained from GOES spacecraft at $135°$ west longitude using the technique of statistical asynchronous regression (O'Brien et al., 2001b). In this technique cumulative probability distributions of electron flux at each hour are calculated. Then it is assumed that the distribution at any hour can be mapped into the distribution at local noon. Mappings for each hour are developed from historical data and are used to transform a time series of observations to a virtual satellite at local noon. We then selected data according to the Russell–McPherron rule corresponding to the four classes of stream interfaces. For each class we superposed the time series of log flux relative to the stream interface and calculated the time variation of the quartiles of log flux. The results are shown in Fig. 12. Clockwise from the upper left the four panels correspond to the four classes identified by the abbreviations II, IE, EE, and EI. In each panel the three traces display the quartiles: upper (red) 75%, middle (green) 50%, and bottom (blue) 25%.

The upper left panel shows the case for both streams ineffective (II) with no persistent sector crossing during the event. In the low-speed stream before the interface the flux is low and decreasing with time. A more rapid drop of flux begins about a day before the interface and reaches a minimum 8 h afterwards. Past the interface the flux increases by about $1\frac{1}{3}$ order of magnitude over a period of 4 days reaching a value about $\frac{1}{2}$ orders of magnitude higher at the end of the plot than was present at the beginning of the plot.
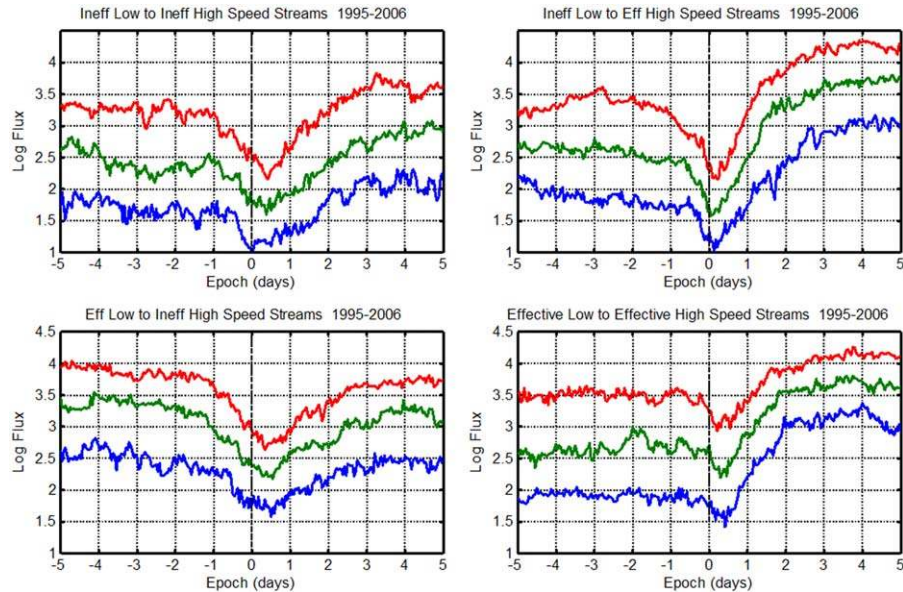
Fig. 12. The behavior of relativistic electrons at synchronous orbit are presented for each of the four classes of CIR. Clockwise from upper left the median flux is shown for the cases II, IE, EE, and EI the three traces represent the three quartiles as a function of epoch time.

The upper right panel shows the transition from ineffective low-speed to effective high-speed (IE) streams. Fluxes at the beginning are comparable to the preceding case, and also decrease toward the interface. Twelve hours before the interface a rapid drop in fluxes begins and at the interface reaches a minimum nearly an order of magnitude below the value at the start of the rapid drop. Immediately after the interface the fluxes increase again reaching a maximum one order of magnitude higher than at the beginning.

The lower right panel presents the effective to effective case (EE). The flux at the beginning of the plot is about the same as in the preceding two cases, but subsequently it increases as the interface approaches (this is an effective low-speed stream). There is a weak drop out ($\frac{1}{2}$ order) associated with the interface and then 6 h later there occurs a 4-day increase to one order of magnitude higher than at the beginning.

The lower left panel shows the transition from an effective low-speed stream to an ineffective high-speed stream (EI). In this case the initial fluxes are the highest of the four cases. They remain high until a rapid drop begins about a day before the interface. The decrease is slightly more than one order of magnitude and the largest of all cases. Twelve hours after the interface the fluxes increase over 4 days to values about $\frac{1}{3}$ order of magnitude lower than the initial values.

These results show that a drop out centered close to the interface is the characteristic behavior of relativistic electrons at synchronous orbit. Another feature is the recovery of electrons by 0.8–2 orders of magnitude after the interface. These results clearly show that substantial acceleration of electrons is more likely when the IMF in the high-speed stream obeys the Russell–McPherron rule. The results also show that electron fluxes can be high and increasing in low-speed streams that satisfy this rule. The most distinct change in flux occurs for transitions from ineffective low-speed streams to effective high-speed streams.

2.11. Statistical occurrence of different classes

The average behavior of relativistic electrons shown in Fig. 12 is summarized in the middle two rows of Table 3. As a simple

measure of the tendency of electrons to decrease before the interface we calculated the difference in median of epoch day -4 and the median of 12 h immediately after the interface. Similarly the tendency to increase after the interface is measured by the difference between the median on day +4 and the same 12-h interval after the interface. Note that both measures are positive numbers. Line three of this table shows that the "no sector change" interfaces (II and EE) have small flux decreases, 0.46 and 0.44, respectively, while those with a sector crossing have greater decreases, 0.64 (IE) and 0.97 (EI). As discussed in Section 3 the total decrease in flux during all CIRs is large compared to that expected from the adiabatic effect of the ring current as measured by Dst (Kim and Chan, 1997). Note in all cases except EI interfaces the increase in flux after the interface exceeds the decrease before. In the exceptional case we suspect that acceleration is present before and absent after the interface.

The increase in fluxes after the interface is ordered differently than the decrease before as demonstrated in line 4 of the table. The smallest increase (0.78) occurs for an EI transition, next is the II interface (0.88), followed by the EE interface (1.37), and finally the IE transition (1.83). The ineffective to effective transition has the next to largest drop before and the largest rise after the interface.

The bottom two rows of Table 3 show the fraction of each class of interface that display anomalous behavior where the changes are opposite to the median behavior. These numbers were determined from full cumulative probability distributions for the changes in each class. The values run between 6.2% and 29.9%. Again, the IE class shows the most consistent behavior with only 6.2% of these interfaces exhibiting a decrease in flux after the interface. The largest anomalous fraction is for the EE transition where nearly a third of the interfaces display an increase in flux before the interface. This is almost certainly a consequence of enhanced activity before the interface.

3. Discussion

In the preceding sections we have demonstrated that the Russell–McPherron effect (Russell and McPherron, 1973) plays an

important role in determining the changes in geomagnetic activity and flux of relativistic electrons associated with a stream interface. The average behavior of the electron fluxes at synchronous orbit without regard for the R–M effect was presented in the center panel of Fig. 9. The flux decreases slowly for several days then shortly before the interface decreases rapidly to a minimum a little after the interface. This is followed by a prolonged increase in flux over a period of about 4 days.

A characteristic feature of the response of relativistic electrons at synchronous orbit to a CIR is a rapid decrease in the flux starting before the stream interface and ending a little after. Averaged over all classes of interfaces the drop out begins 12–24 h before the interface and ends 6 h after. However, as shows in Fig. 12 the details of this response depend on the class of interface. The behavior is most pronounced for the transition from an ineffective low-speed stream to an effective high-speed stream (IE). For this class of CIR the flux decreases by nearly a factor of 10 beginning 12 h before the interface and ending at the interface. For the EE transition the drop out begins at the interface and ends about 8 h later. For this case the decrease in median flux is only a factor of 2. The transition from either effective or ineffective low-speed streams to ineffective high-speed streams (II and EI) is less sharp, longer in duration, and fairly large. In both cases the drop out begins nearly a day before the interface and ends about 6 h after the interface and the decrease in nearly a factor of 10.

One of the first explanations for the drop out of electron fluxes is the "Dst Effect" of magnetic storms described by Kim and Chan (1997). Conservation of all three adiabatic invariants of the electrons as a ring current slowly grows (decreasing Dst) causes an electron to move radially outward in the magnetosphere and lose energy. At synchronous orbit the electron flux at a specific energy decreases proportional to the ratio of the final magnetic field to the initial magnetic field along the inner orbit. Electrons initially at synchronous orbit move further out in the magnetosphere and depending on the standoff distance of the magnetopause may be permanently lost through the dawn magnetopause. If the solar wind dynamic pressure is weak this will not happen and the electrons should reappear at synchronous orbit when the ring current decays.

In our case the Dst effect is unlikely to be the explanation for the observed flux drop out. First, the timing of the decrease is wrong for at least three classes of CIR (all but EE). In these three cases the flux decrease begins 12–24 h before the interface, but the storm main phase (Dst decrease) occurs after the interface. Second, the magnitude of the decrease in fluxes is too large for the size of the magnetic storms (Figs. 11 and 12). For ineffective high-speed streams the minimum median Dst is greater than -20 nT. According to Kim and Chan (1997) (their Fig. 5) the decrease expected for this value of Dst is about $\frac{1}{10}$ of a decade. For effective high-speed streams minimum median Dst is ~-30 nT and the expected decrease is $\frac{2}{10}$ of a decade. The observed decrease is close to a full decade, much larger than predicted. Note, however, it is possible that the smaller flux decrease after the interface in three of the cases (all but IE) could be attributed to this effect as the timing and magnitude are closer to expectations.

If not the Dst effect then what is the cause of the flux decreases? The rapid flux decreases typically begin 12–24 h before the interface. In the solar wind the early part of this interval is characterized by low solar wind velocity, a significant westward deflection of the azimuthal flow angle, a gradually increasing dynamic pressure, and an increase in the magnitude of the IMF. On the ground PC 5 wave power begins to increase during this interval. In the later part of the interval large negative fluctuations in gsm Ey are observed. The compression of the magnetic field by the solar wind may increase the perpendicular anisotropy of both electrons and protons leading to stronger pitch angle scattering into the loss cone. Inward motion of the magnetopause may result in the loss of some electrons beyond synchronous orbit through the dawn magnetopause. Outward radial diffusion by ULF waves might then contribute to the magnetopause loss process. Somewhat later southward fluctuations in IMF Bz amplified by the compression inside the CIR may generate bursts of convection and the creation of plasmapause plumes in the late afternoon sector. Protons with an anisotropic pitch angle distribution drift westward into these plumes and then as discussed by Summers and Thorne (2003) ion cyclotron waves are generated. When relativistic electrons drift though these waves they experience rapid pitch angle scattering and are lost to the ionosphere.

The current model to explain the acceleration of electrons consists of a number of distinct processes (Friedel et al., 2002). A southward turning of the IMF initiates dayside reconnection and transport of magnetic flux to the tail. Plasma-carrying magnetic flux begins to convect out of the tail to the dayside thinning the plasma sheet and its embedded current sheet. Additional thinning is caused by the enhanced magnetic pressure in the tail lobes. Eventually the tail current sheet becomes thin enough for magnetic reconnection to begin in some localized region. At the reconnection site plasma and magnetic flux are accelerated earthward in a narrow channel. Electric fields associated with this earthward collapse of the field accelerate electrons and inject them in the outer magnetosphere. North–south fluctuations of the IMF cause a sequence of these events (magnetospheric substorms). Electrons are injected into the inner magnetosphere both by background convection and by the plasma jets associated with each of these substorms.

The injected electrons have a power law spectrum with very few particles at relativistic energies (Baker et al., 1998). The electrons drift eastward in the magnetosphere producing VLF waves through various instabilities. Depending on pitch angle and energy, and the background plasma, different types of waves scatter electrons either in pitch angle (loss to atmosphere) or energy (acceleration) (Millan and Thorne, 2007). Protons injected in conjunction with the electrons drift westward and interact with plasma plumes created by fluctuations in the convection electric field. The interaction produces ion cyclotron waves that also scatter lower energy electrons in pitch angle (loss to atmosphere) (Loto'aniu et al., 2006). In our current work we did not examine ion cyclotron wave occurrence or the existence of plasma plumes. However, in an old paper (McPherron and Ward, 1967) we demonstrated that there is a very high probability of observing pearl pulsations (structured Pc 1) for several days after the passage of an IMF sector when Kp exceeds 4. In results not presented here we find that Kp satisfies these conditions for about 2 days after a stream interface so it is likely that ion cyclotron waves play a role in relativistic electron dynamics during the passage of CIRs. Clearly further study of this question with modern data is warranted.

ULF waves in the Pc 5 band may also play a role in the acceleration or loss of relativistic electrons through drift resonance (Elkington et al., 1999; Elkington et al., 2003). As we showed in Fig. 9 the behavior of ULF waves mimics the changes in solar wind velocity suggesting that they are generated by the Kelvin–Helmholtz instability at the magnetopause. A recent study by Claudepierre et al. (2008) uses an MHD simulation to investigate how K–H waves are produced in the low-latitude boundary layer during southward IMF and demonstrates that these waves can interact with several hundred keV electrons. If the phase space density of electrons decreases inward Pc 5 waves will scatter a fraction of the electrons inward conserving their first invariant so that they gain energy. If on the other hand, the phase space density is peaked inside synchronous orbit ULF waves might move electrons outward past synchronous orbit contributing to

loss through the magnetopause. If all of these processes persist for several days, and acceleration dominates loss, a fraction of the injected electrons are scattered to relativistic energy and their flux measured at synchronous orbit increases.

The role of CIRs and the stream interfaces separating the slow- and high-speed solar wind is to organize and maintain the processes within the magnetosphere for a sufficient length of time that a substantial number of electrons are accelerated to relativistic energy (Lyons et al., 2005). First consider the situation near summer and winter solstice. At this time the Russell–McPherron effect does not operate. Nonetheless a CIR can still produce relativistic electrons. In the slow-speed wind before the interface, the IMF is stable in the ecliptic plane and the velocity of the solar wind is low. As a consequence Ey applied to the magnetosphere is weak and there is little convection and few substorms. The processes described above either do not occur or are very weak. The flux of relativistic electrons is everywhere decaying. When the edge of the CIR passes Earth the dynamic pressure of the solar wind begins to increase. This reduces the size of the magnetosphere and electrons near the magnetopause are lost to the magnetosheath. Other electrons are redistributed in the magnetosphere to maintain their adiabatic invariants. This is the beginning of the rapid decrease of about a factor of 10. After the interface passes compressed IMF and higher speed increase the relativistic electron flux by about a factor of 30 to a level about 20 times lower than seen in geoeffective streams around equinox.

As the stream interface passes, Earth is imbedded in the high-speed stream so that any southward fluctuation in the IMF is amplified by the high velocity, and convection and substorms are enhanced. Equally important is the fact that immediately behind the stream interface the solar wind is filled with large amplitude Alfvén waves of 1–3 h period propagating away from the Sun (Tsurutani and Ho, 1999). Each time a wave turns the IMF southward a substorm results and particles are injected into the inner magnetosphere. Since the waves persist for several days the acceleration processes described above are continually present and accelerate a large number of electrons to relativistic energies. The process is assisted by the continued presence of Pc 5 waves generated on the magnetopause and by substorms.

At equinoxes the Russell–McPherron effect becomes important. If the low-speed stream is ineffective by the rule "Spring To Fall Away", IMF Bz in gsm coordinates has a positive bias and even with fluctuations the IMF is predominantly northward causing substorm activity to be at a minimum. This allows loss processes to dominate acceleration and relativistic electron fluxes decrease. If there is an IMF sector crossing just before the interface the high-speed stream following the interface will be geoeffective. The gsm Bz of the IMF will be biased southward and substorm activity will be stronger and persist for longer intervals. This enhances the internal processes that accelerate electrons. The result of this transition is a dramatic contrast in fluxes before and after the interface.

The situation is very different for an effective to ineffective (EI) stream interface. Weak activity caused by a southward bias of gsm Bz before the interface counteracts the loss of electrons. After the interface the IMF is biased northward and the substorms caused by the IMF fluctuations are weaker. The electron fluxes never recover to the level they had before the interface. The ineffective to ineffective (II) stream interface produces far fewer electrons than other classes since the IMF is biased northward in both streams. The effective to effective stream interface has electron fluxes constant or increasing during the low-speed stream, a small drop out at the interface, and then substantial acceleration after the interface.

The knowledge that the Russell–McPherron effect plays an important role in acceleration of relativistic electrons might be used by space weather forecasters. The maps of the cumulative probability distributions of electron fluxes allow one to predict the probability they will exceed a certain level at various times relative to the interface (McPherron and Siscoe, 2004; McPherron et al., 2004). To accomplish this it is necessary to predict when the interface will arrive and the orientation of the IMF in the low- and high-speed streams. Present models of the solar wind based on the potential field expansion of the coronal fields are quite good in predicting the solar wind velocity at Earth and the polarity of the IMF (Arge and Pizzo, 2000; Odstrcil et al., 2004). They are not so good at determining whether an IMF sector crossing will precede the stream interface. Observations in the slow-speed stream will help, and if a transition is observed prior to the interface it is possible to predict the future behavior provided the polarity of the IMF remains fixed. An alternative approach is to use observations of the solar wind and IMF at a spacecraft following Earth in Earth orbit (Stereo B). CIRs and stream interfaces will arrive at such a spacecraft earlier than Earth and the measured properties can be used to predict what will be seen at Earth a short time later.

Acknowledgments

References

Arge, C.N., Pizzo, V.J., 2000. Improvement in the prediction of solar wind conditions using near-real time solar magnetic field data. Geophys. Res. Lett. 105 (A5), 10,465–10,479.

Baker, D., et al., 1990. Linear prediction filter analysis of relativistic electron properties at 6.6 Re. J. Geophys. Res. 95 (A9), 15133–15140.

Baker, D., et al., 1999a. Equinoctial and solstitial averages of magnetospheric relativistic electrons: a strong semiannual modulation. Geophys. Res. Lett. 26 (20), 3193–3196.

Baker, D.N., et al., 1986. Highly relativistic electrons in the earth's outer magnetosphere 1. Lifetimes and temporal history 1979–1984. J. Geophys. Res. 91 (A4), 4265–4276.

Baker, D.N., et al., 1989. Relativistic electrons near geostationary orbit: evidence for internal magnetospheric acceleration. Geophys. Res. Lett. 16 (6), 559–562.

Baker, D.N., et al., 1998. Strong electron acceleration in the earth's magnetosphere. Adv. Space Res. 21 (4), 609–613.

Baker, D.N., et al., 1999b. Equinoctial and solstitial averages of magnetospheric relativistic electrons: a strong semiannual modulation. Geophys. Res. Lett. 26 (20), 3193–3196.

Bargatze, L.F., et al., 2005. A new interpretation of Weimer et al.'s solar wind propagation delay technique. J. Geophys. Res. 110 (A7), 1–12.

Claudepierre, S.G., et al., 2008. Solar wind driving of magnetospheric ULF waves: pulsations driven by velocity shear at the magnetopause. J. Geophys. Res. 113 (A5), 1–16.

Cliver, E.W., et al., 2000. Mountains versus valleys: semiannual variation of geomagnetic activity. J. Geophys. Res. 105 (A2), 2413–2424.

Crooker, N.U., Siscoe, G.L., 1986. The effect of the solar wind on the terrestrial environment. In: Sturrock, P.A. (Ed.), Physics of the Sun. D. Reidel, pp. 193–249.

Elkington, S., et al., 1999. Acceleration of relativistic electrons via drift-resonant interaction with toroidal-mode Pc-5 ULF oscillations. Geophys. Res. Lett. 26 (21), 3273–3276.

Elkington, S.R., et al., 2003. Resonant acceleration and diffusion of outer zone electrons in an asymmetric geomagnetic field. J. Geophys. Res. 108 (A3) SMP11-11–SMP11-15.

Forsyth, R.J., Marsch, E., 1999. Solar origin and interplanetary evolution of stream interfaces. Space Sci. Revs. 89 (1–2), 7–20.

Friedel, R.H.W., et al., 2002. Relativistic electron dynamics in the inner magnetosphere—a review. J. Atmos. Sol.-Terr. Phys. 64 (2), 265–282.

Gonzalez, W.D., et al., 1994. What is a geomagnetic storm? J. Geophys. Res. 99 (A4), 5771–5792.

Gosling, J., et al., 1978a. Solar wind stream interfaces. J. Geophys. Res. 83 (A4), 1401–1412.

Gosling, J.T., et al., 1978b. Solar wind stream interfaces. J. Geophys. Res. 83 (A4), 1401–1411.

Gosling, J.T., Pizzo, V.J., 1999. Formation and evolution of corotating interaction regions and their three dimensional structure. Space Sci. Revs. 89 (1–2), 21–52.

Haaland, S., et al., 2006a. Comment on "A new interpretation of Weimer et al.'s solar wind propagation delay technique" by Bargatze et al. J. Geophys. Res. 111 (A06102).

Haaland, S., et al., 2006b. Comment on "A new interpretation of Weimer et al.'s solar wind propagation delay technique"; by Bargatze et al. J. Geophys. Res. 111 (A6), 1–4.

Horne, R.B., et al., 2006. Mechanisms for the acceleration of radiation belt electrons. In: Tsurutani, B., et al. (Eds.), Corotating Solar Wind Streams and Recurrent Geomagnetic Activity. American Geophsical Union, Washington, DC.

Hundhausen, A.J., 1977. An interplanetary view of coronal holes. In: Zirker, J.B. (Ed.), Coronal Holes and High Speed Wind Streams. Colo. Assoc. University Press, Boulder, pp. 225–329.

Kim, H.-J., Chan, A., 1997. Fully adiabatic changes in storm time relativistic electron fluxes. J. Geophys. Res. 102 (A10), 22107–22116.

Li, X., et al., 2001. Long term measurements of radiation belts by SAMPEX and their variations. Geophys. Res. Lett. 28 (20), 3827–3830.

Loto'aniu, T.M., et al., 2006. Estimating relativistic electron pitch angle scattering rates using properties of the electromagnetic ion cyclotron wave spectrum. J. Geophys. Res. A—Space Phys. 111 (A4), 11.

Lyons, L.R., et al., 2005. Solar wind–magnetosphere coupling leading to relativistic electron energization during high-speed streams. J. Geophys. Res. A–Space Phys. 110 (A11), 9.

McPherron, R.L., Siscoe, G., 2004. Probabilistic forecasting of geomagnetic indices using solar wind air mass analysis. Space Weather 2 (1), 1–10.

McPherron, R.L., Ward, S.H., 1967. Correlation between occurrence of pearl pulsations and interplanetary magnetic field sector boundaries. J. Geophys. Res. 72 (1), 393–398.

McPherron, R.L., et al., 2004. Probabilistic forecasting of the Dst index. In: T.I. Pulkkinen, etal. (Ed.), The Inner Magnetosphere: Physics and Modeling. American Geophysical Union, Helsinki, Finland, pp. 203–210.

Millan, R.M., Thorne, R.M., 2007. Review of radiation belt relativistic electron losses. J. Atmos. Sol.-Terr. Phys. 69 (3), 362–377.

Nagai, T., 1988. "Space weather forecast": prediction of relativistic electron intensity at synchronous orbit. Geophys. Res. Lett. 15 (5), 425–428.

Ness, N.F., Wilcox, J.M., 1965. Sector structure of the quiet interplanetary magnetic field. Science 18, 1592–1594.

O'Brien, T.P., et al., 2001a. Which magnetic storms produce relativistic electrons at geosynchronous orbit? J. Geophys. Res. 106 (A8), 15533–15544.

O'Brien, T.P., et al., 2001b. Statistical asynchronous regression: determining the relationship between two quantities that are not measured simultaneously. J. Geophys. Res. 106 (A7), 13247–13259.

Odstrcil, D., et al., 2004. Initial coupling of coronal and heliospheric numerical magnetohydrodynamic codes. J. Atmos. Sol.-Terr. Phys. 66 (15–16), 1311–1320.

Paulikas, G.A., Blake, J.B., 1979. Effects of the solar wind on magnetospheric dynamics: energetic electrons at the synchronous orbit. In: Olsen, W.P. (Ed.), Quantitative Modeling of Magnetospheric Processes. American Geophysical Union, Washington, DC, pp. 180–202.

Phillips, J., et al., 1995. Ulysses solar wind plasma observations from pole to pole. Geophys. Res. Lett. 22 (23), 3301–3304.

Reeves, G., 1998. Relativistic electrons and magnetic storms: 1992–1995. Geophys. Res. Lett. 25 (11), 1817–1820.

Reeves, G.D., et al., 2003. Acceleration and loss of relativistic electrons during geomagnetic storms. Geophys. Res. Lett. 30 (10), 36-31–36-34.

Roberts, D.A., Goldstein, M.L., 1990. Do interplanetary Alfven waves cause auroral activity? J. Geophys. Res. 95 (A4), 4327–4331.

Rostoker, G., et al., 1998. On the origin of relativistic electrons in the magnetosphere associated with some geomagnetic storms. Geophys. Res. Lett. 25 (19), 3701–3704.

Russell, C.T., McPherron, R.L., 1973. Semiannual variation of geomagnetic activity. J. Geophys. Res. 78 (1), 92–108.

Summers, D., Thorne, R.M., 2003. Relativistic electron pitch-angle scattering by electromagnetic ion cyclotron waves during geomagnetic storms. J. Geophys. Res. 108 (A4) SMP2-1–SMP2-12.

Tsurutani, B.T., Gonzalez, W.D., 1987. The cause of high-intensity long-duration continuous $<i>AE</i>$ activity (HILDCAAs): interplanetary Alfven wave trains. Planet. Space Sci. 35 (4), 405–412.

Tsurutani, B.T., Ho, C.M., 1999. A review of discontinuities and Alfven waves in interplanetary space: Ulysses results. Rev. Geophys. 37 (4), 517–541.

Weimer, D.R., 2004. Correction to "Predicting interplanetary magnetic field (IMF) propagation delay times using the minimum variance technique. J. Geophys. Res., 109, A12104, doi:10.1029/2004JA010691.

Weimer, D.R., et al., 2003. Predicting interplanetary magnetic field (IMF) propagation delay times using the minimum variance technique. J. Geophys. Res. 108 (A1) SMP16-11–SMP16-12.

Wilcox, J., Ness, N.F., 1965. Quasi-stationary corotating structure in the interplanetary medium. J. Geophys. Res. 70 (23), 5793–5805.

Williams, D.J., 1966. A 27-day periodicity in outer zone trapped electron intensities. J. Geophys. Res. 71 (7), 1815–1826.